*Acta Oceanol. Sin.*, 2020, Vol. 39, No. 11, P. 21–32
https://doi.org/10.1007/s13131-020-1677-y
http://www.hyxb.org.cn
E-mail: hyxbe@263.net

# Surface water exchanges in the Luzon Strait as inferred from Lagrangian coherent structures

Zhehao Zheng[1], Wei Zhuang[1, 2]*, Jianyu Hu[1, 2], Zelun Wu[1, 3], Changjian Liu[4]

[1] State Key Laboratory of Marine Environmental Science, College of Ocean and Earth Sciences, Xiamen University, Xiamen 361102, China

[2] Southern Marine Science and Engineering Guangdong Laboratory (Zhuhai), Zhuhai 519082, China

[3] Joint Center for Ocean Remote Sensing, University of Delaware-Xiamen University, Newark, DE 19716, USA

[4] South China Sea Marine Survey and Technology Center, Ministry of Natural Resources, Guangzhou 510300, China

Received 1 May 2020; accepted 10 August 2020

**Abstract**

This study presents a Lagrangian view of upper water exchanges across the Luzon Strait based on the finite-time Lyapunov exponents (FTLE) fields computed from the surface geostrophic current. The Lagrangian coherent structures (LCSs) extracted from the FTLE fields well identify the typical flow patterns and eddy activities around the Luzon Strait. In addition, they reveal the intricate transport paths and fluid domains, which are validated by the tracks of satellite-tracked surface drifters and cannot be visually recognized in the velocity maps. The FTLE fields indicate that there are mainly four types of transport patterns near the Luzon Strait; among them, the Kuroshio northward-flowing “leaping” pattern and the clockwise rotating “looping” pattern occur more frequently than the “leaking” pattern of the direct Kuroshio branch into the SCS and the “outflowing” pattern from the SCS to the Pacific. The eddy shedding events of the Kuroshio at the Luzon Strait are further analyzed, and the importance of considering LCSs in estimating transport by eddies is highlighted. The anticyclonic eddy (ACE) shedding cases reveal that ACEs mainly originate from the looping paths of Kuroshio and thus could effectively trap the Kuroshio water before eddy detachments. LCSs provide useful information to predict the positions of the upstream waters that finally enter the ACEs. In contrast, LCS snapshots indicate that during the formation of cyclonic eddies (CEs), most CEs are not connected with the pathways of Kuroshio water. Hence, the contribution of CEs to the surface water exchanges from the Pacific into the SCS is tiny.

**Key words:** Lagrangian coherent structures (LCSs), Kuroshio, Luzon Strait, transport pathways, particle tracking

**Citation:** Zheng Zhehao, Zhuang Wei, Hu Jianyu, Wu Zelun, Liu Changjian. 2020. Surface water exchanges in the Luzon Strait as inferred from Lagrangian coherent structures. Acta Oceanologica Sinica, 39(11): 21–32, doi: 10.1007/s13131-020-1677-y

## 1 Introduction

The Kuroshio is the poleward western boundary current of the North Pacific subtropical gyre. It mainly originates from the westward flowing North Equatorial Current, which bifurcates at the eastern coast of the Philippine Archipelago. The Kuroshio then flows northeastward, passing by the Luzon Strait, Taiwan Island, and Ryukyu Islands.

The South China Sea (SCS), which is the largest semienclosed marginal sea in the northwestern Pacific, is characterized by East Asian monsoon climate and a complex geometry (Fig. 1). A number of straits connect the SCS with the adjacent waters. Among these straits, the Luzon Strait is the only deep (>2 200 m) passage, and it is also the major oceanic pathway between the SCS and the Pacific Ocean. Over several decades, it has been observed that when the Kuroshio passes by the Luzon Strait, a portion of the warm and salty Pacific water enters the SCS (Shaw, 1991; Qu et al., 2000; Zhu et al., 2019). In the sense of annual mean, the inflow through the Luzon Strait partially flows out of the SCS through the Karimata and Mindoro Straits, forming the so-called SCS throughflow that is important for the heat and salt budgets of the SCS basin (Qu et al., 2005, 2006; Wang et al., 2006; Fang et al., 2009; Gordon et al., 2012; Wei et al., 2019).

With regard to the upper layer, both the historical hydrographic data and the surface drifter trajectories indicate notable seasonality of surface water exchange through the Luzon Strait (Shaw, 1991; Centurioni et al., 2004). The surface Kuroshio intrusion into the SCS is the largest in winter, followed by that in spring and in autumn; however, there is still no consensus on whether the water exchange in summer flows westward into the SCS or eastward into the northwestern Pacific Ocean (Shaw, 1991; Chu and Li, 2000). High-resolution satellite images reveal that the surface Kuroshio path in the Luzon Strait shows significant transient features and appears to be closely related to the nearby eddy activities (Yuan et al., 2006; Nan et al., 2011; Qiu et al., 2019; Zheng et al., 2019). Further, the unstable nature of the Kuroshio intrusion has been verified by model simulations (Metzger and Hurlbert, 2001; Xue et al., 2004), and the intruding path can be roughly divided into three types: the looping path, leaping path, and leaking path (Nan et al., 2011, 2015). Because of the complexity of the dynamic environment and the nondeterministic nature of flow pattern around the Luzon Strait, the variability of flow trajectories and the relevant dynamics are still not well

---

Foundation item: The National Key Research and Development Program of China under contract No. 2016YFA0601201; the National Natural Science Foundation of China under contract Nos 91858202, 91958203, 41730533 and 41776003.

*Corresponding author, E-mail: wzhuang@xmu.edu.cn

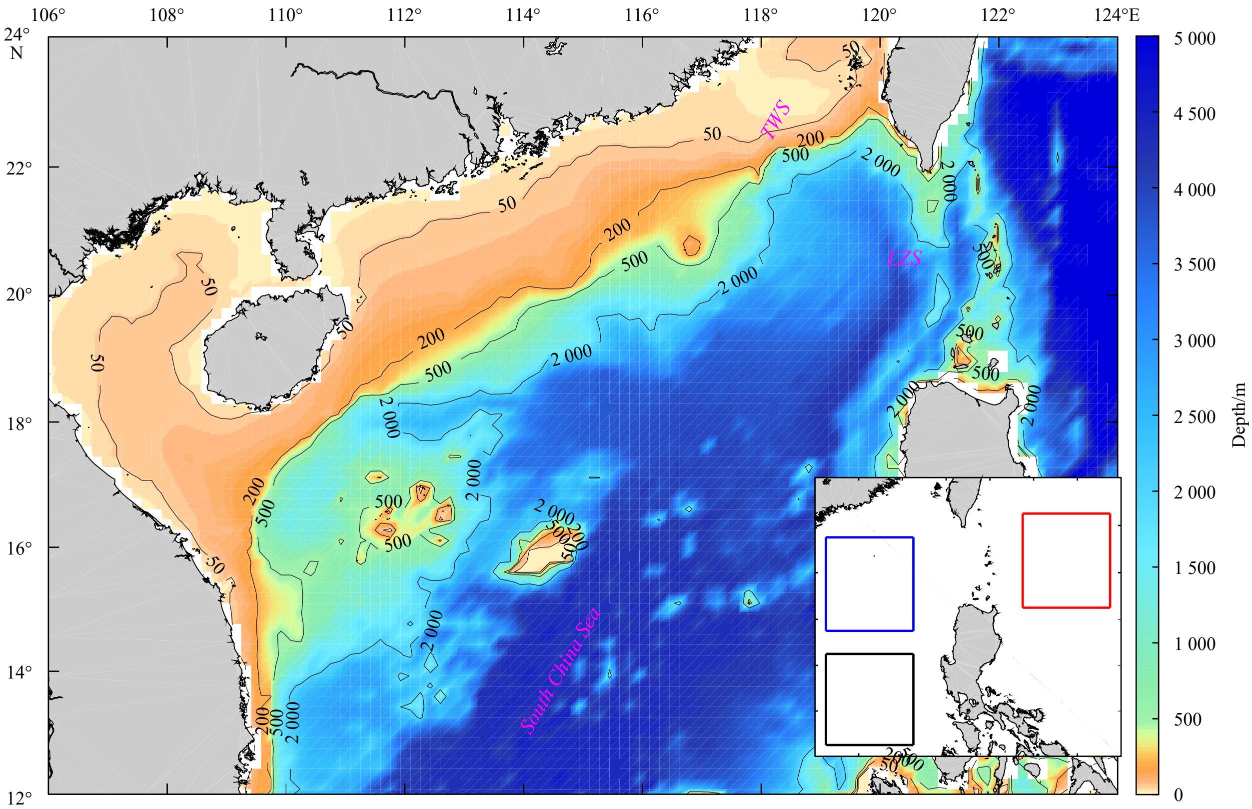

**Fig. 1.** Topography around the northern South China Sea. The blue, black, and red boxes in the inset are the northern and central areas of the SCS and the northwest Pacific regions, respectively, considered for calculating the regional averages shown in Fig. 10. TWS and LZS denote the Taiwan Strait and the Luzon Strait, respectively.

understood.

Rich eddies have also been observed near the Luzon Strait by both hydrographic observations and satellite altimeter data (e.g., Li et al., 1998; Wang et al., 2003; Wang et al., 2019). Anticyclonic eddy (ACE) sheddings from the Kuroshio Current loop (KCL) are considered to be one of the most important processes of eddy formation in the northern SCS (Jia and Chassignet, 2011; Zhang et al., 2017). The detached ACEs could effectively trap warm and salty Pacific water and transport it westward into the interior SCS (Zhang et al., 2017). The spatiotemporal evolutions of mesoscale eddies in the SCS have been described by different kinds of eddy detection algorithms, most of which are based on the Eulerian point of view (e.g., Lian et al., 2019). Unlike the widely used Eulerian-based approaches, Li et al. (2011) proposed a distinctive eddy identification method in a Lagrangian framework, which captured both the mesoscale and submesoscale eddies in the SCS from the surface drifter trajectories. The advantages of Lagrangian approaches have also been extended to the estimation of diffusivities and their related time and length scales in the SCS (Qian et al., 2013).

Although the traditional particle tracking analysis does yield the full trajectory histories of individual fluid parcels, the trajectories are often sensitive to small changes in the time and location of release (Haller, 2015). Thus the convoluted "spaghetti plots" of trajectories are sometimes difficult to interpret. In recent years, the concept of Lagrangian coherent structures (LCSs) provide an alternative way in the Lagrangian sense to better understand why fluid elements evolve the way they do (Haller and Yuan, 2000; Wiggins, 2005; Branicki and Wiggins, 2009). Ideally, LCSs can be regarded as material lines, with the locally strongest repelling or attracting natures. Thus, they delineate the boundaries between fluid domains with quite distinct advection characteristics, which cannot be revealed by a visual inspection of velocity field snapshots. In addition, the dynamical "skeletons" of flows unfolded by LCSs can keep unchanged for any choice of reference frame. This is different from traditional Eulerian descriptions, such as streamlines, vorticity or other frame-dependent quantities, which do not remain invariant under different reference frames (Peacock and Haller, 2013). At present, LCSs are widely applied in ocean sciences for purposes such as predicting the movement of oil spill (Lehahn et al., 2007; Peacock and Haller, 2013), clarifying the horizontal advection of river runoff near the estuaries (Huhn et al., 2012; Wei et al., 2018), and estimating the intensity of ocean mixing (D'Ovidio et al., 2004). Huang et al. (2015) illustrated the LCSs near the Luzon Strait and depicted two dominant patterns: Southeast-northwest orientated LCSs in winter and southwest-northeast LCSs in summer. But this work did not discuss the transport structures in spring and autumn seasons. Moreover, as a typical pattern in the Luzon Strait, the KCL and the relevant eddy sheddings have not been investigated in this work as well.

In order to have a more complete understanding of the surface water exchanges through the Luzon Strait, this study utilizes the data of satellite-tracked surface drifters and the LCSs obtained from the integrated velocity fields to characterize the regional variability of transport pathways and barriers on intraseasonal, seasonal and interannual timescales. The rest of this paper is organized as follows: Section 2 briefly describes the data and methods used in this work. The concept of LCSs is the key point described in this section. Section 3 presents different types of typical flow patterns around the Luzon Strait as inferred from the LCSs. Here, greater attention has been paid to the events of eddy shedding from the Kuroshio into the SCS and the entrainment of Kuroshio water during eddy formation. Section 4 provides the discussion and summary.

## 2 Data and methods

### 2.1 *Data*

The surface geostrophic velocities adopted in this study are provided by the Copernicus Marine and Environment Monitoring Service (CEMES) based on satellite and *in situ* observations. The geostrophic currents are computed for latitudes beyond ±5° from the absolute dynamic topography fields, which are obtained by adding the sea level anomalies observed by all available satellite altimeter missions to a mean dynamic topography (Pujol et al., 2016). In this study, we used the geostrophic current data with a 0.25°×0.25° spatial grid and 1-d time interval during the period 1993–2017. The altimeter observations over the shallow shelf could be contaminated by aliasing errors due to high-frequent tide and atmospheric forcing. Therefore, this study mainly focuses on the areas deeper than 200 m where the sea level data reach centimetric accuracy, although the results near coastal regions are also plotted.

The LCSs computations were validated using the satellite-tracked drifter data obtained from the NOAA/AOML Drifter Data Assembly Center. This study only uses the results from drifters with drogues centered at 15-m depth. Compared with the trajectories of undrogued drifters, the results from drogued drifters are less affected by the wind-generated slip and thus better reflect the near-surface ocean current (Lumpkin and Johnson, 2013). The positions of each drifter were interpolated in 6-h intervals and could well reflect the trajectories of near-surface water particles. The period selected for drifter data was from 2000 to 2017.

*In situ* temperature and salinity profiles sampled by conductivity-temperature-depth (CTD) profilers during two cruises in January 2010 and May 2017 were also used to describe the water mass characteristics within different eddies. The oceanographic survey on January 16–31, 2010 was carried out by the South China Sea Engineering Survey Center in the continental shelf and slope waters in the northern SCS. It captured the center of a strong ACE at about 20.75°N, 118°E (Liu et al., 2013). Another cruise mission was conducted in the northeastern SCS during the period May 23–25, 2017, and obtained CTD measurements at 15 stations (Huang et al., 2019). The cruise transect crossed the northern part of a well-developed cyclonic eddy (CE), where three CTD profiles were sampled at 21°N, 118.5°–119°E. More details about these two hydrographic surveys are presented in the reports of Liu et al. (2013) and Huang et al. (2019).

### 2.2 *Methods*

In this study, we utilized the finite-time Lyapunov exponent (FTLE) to locate LCSs. The FTLE is the finite-time average of the maximum expansion or contraction rate for neighboring passive fluid particles. The method of extracting LCSs from FTLE fields has been widely used in previous studies (e.g., Shadden et al., 2005; Beron-Vera et al., 2008). Physically, the FTLE is a scalar measure of the finite-time separation rate of neighboring fluid particles.

The mathematical expression for FTLE is as follows:

$$\sigma_{t_0}^{T}(x_0) = \frac{1}{|T|}\ln \| \partial_{x_0} x(t_0 + T; t_0, x_0) \| , \qquad (1)$$

where $\| \ \|$ denotes the matrix norm, and $x\,(t_0{+}T;\ t_0,\ x_0)$ represents at the time $t{=}t_0{+}T$ the position of a fluid parcel, which is at $x_0$ at the initial time $t{=}t_0$. As a scalar field in space, the FTLE is obtained by time integration of the velocity fields. The ridges identified by forward-integrated ($t{>}0$) and backward-integrated ($t{<}0$) FTLE fields are called repelling and attracting LCSs, respectively. Therefore, partition a fluid domain into some coherent subsets with different advective dynamics. Compared with the typical oceanic diagnostics based on the Eulerian view, the Lagrangian method can provide more detailed information of ocean characteristics, even on some scales smaller than the spatial resolution of velocity fields. Moreover, the FTLE fields are computed based on time-dependent flow fields. Hence, they are not as sensitive to individual abnormal data in some flow fields as the Eulerian variables and thus are more robust (Haller, 2001; Shadden et al., 2005).

In this work, the FTLE fields were produced by advecting artificial tracers for a finite timescale in the space with a resolution 10 times finer than the velocity grid, which can reveal great detail of LCSs. The tracer trajectories were determined using a fourth-order Runge–Kutta method and a linear interpolation of the surface velocities to tracer positions in time and space. The total length of time integral was 35 d, and the time step was set to 0.5 d. It is found that the FTLE results are insensitive to the both spatial and temporal resolutions of velocity fields and the interpolation methods (Harrison and Glatzmaier, 2010). The length of time integral is a key parameter for deriving meaningful FTLE fields. A much shorter timescale may hinder the tracers to depict the whole LCS structure, while the tracers integrated for a much longer timescale could map some different parts of the flow. The choice of 35 d for time integral was the same as Andrade-Canto et al. (2013), which investigated the Loop Current eddy separations in the Gulf of Mexico and was similar to the present study in terms of spatial scales and dynamic processes. Sensitivity tests further showed that the patterns of FTLE did not alter notably when the integration time changed from 30 d to 40 d (figures not shown). In the adopted FTLE algorithm, tracers stopped integrating when they reached the boundary. In this case, there may exist some errors near the boundaries. Therefore, we selected a relatively large calculation domain (5°–30°N, 105°–130°E) to keep the key region of interest far away from the boundaries. Given our focus on identifying the transport pathways, the FTLE fields discussed below refer to the results of time backward integration, unless otherwise specified.

## 3 Results

### 3.1 *Validation of LCSs based on the satellite-tracked surface drifters*

Figure 2 shows the time backward FTLE fields from October 11 to 19, 2003, and the instantaneous positions of 11 satellite-tracked drogue drifters on the same dates. The regions with intense red tones indicate the LCSs defined by the ridges with the maximum FTLE values. The movements of drifters generally followed the identified ridges in the FTLE fields. Specifically, 10 of 11 drifters marched clockwise along the circular lines of ridges indicative of the existence and trapping effect of an ACE to the east of the Kuroshio. The only exception was the southernmost drifter on October 11; it moved westward until October 15 along another channel composed of FTLE ridges outside the eddy and finally joined the northward-flowing Kuroshio mainstream. The good correspondence between the movement of drifters and the FTLE fields validates the ability of LCSs to reflect

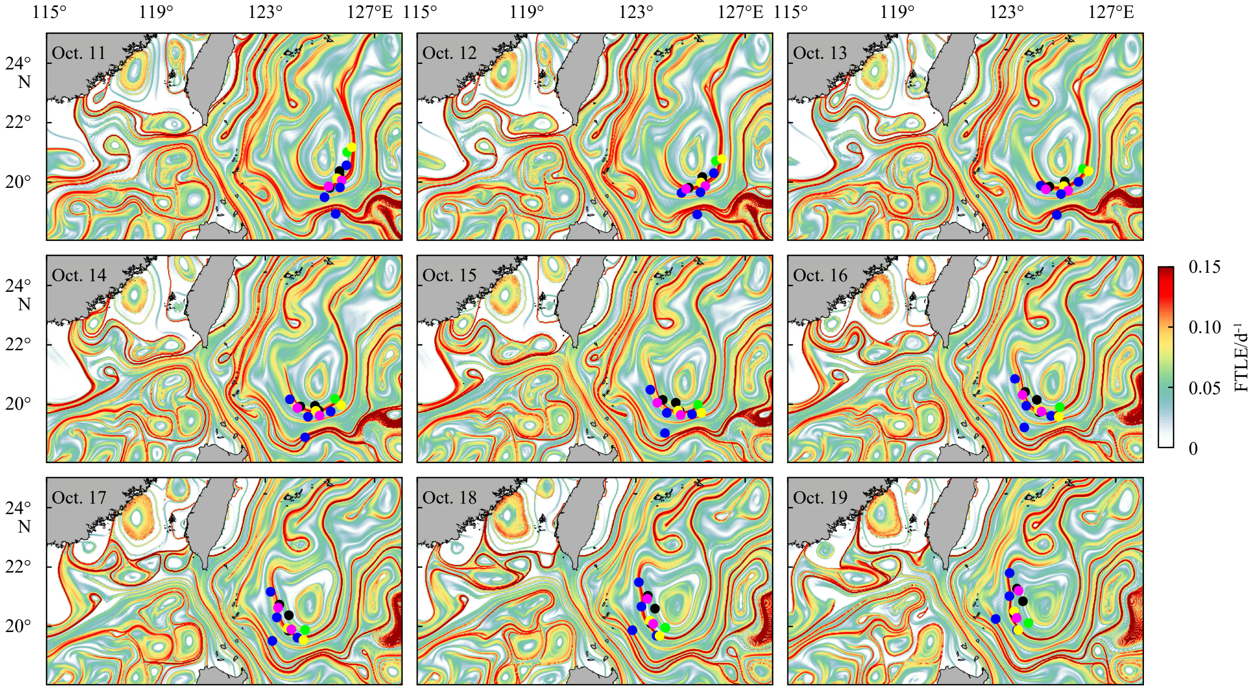

**Fig. 2.** Snapshots of the finite-time Lyapunov exponents (FTLE) fields from October 11 to 19, 2003. Overlaid on each FTLE field is the instantaneous positions of 11 satellite-tracked drifters.

the transport trajectories and barriers in the study area.

### 3.2 *Statistical characteristics of four major LCS types*

According to the tracks of drogue drifters from 2000 to 2017, the flow exchanges through the Luzon Strait can be mainly classified into four categories. The first type shows the northwestward flowing “leaking” pattern of Kuroshio, in which most of drifters directly intrude into the SCS and flow southwestward following the SCS western boundary current (Fig. 3e). The FTLE field on March 8, 2003, represents a typical Kuroshio leaking pattern with the LCSs extending northwestward from east of Luzon Island into the SCS (Fig. 3a). Interestingly, in contrast to the continuous FTLE ridges along the Kuroshio mainstream east of Luzon Strait and Taiwan Island, the Kuroshio branches into the SCS often show more complex discontinuous patterns that probably arise from the local enhanced instabilities and mixing (e.g., Zhuang et al., 2010; Wang et al., 2017). The second type is the northward “leaping” pattern of Kuroshio. This pattern is characterized by northward moving drifters leaping across the Luzon Strait (Fig. 3f). A corresponding FTLE field on March 31, 2003 (Fig. 3b) exhibits LCSs along the Kuroshio path spreading northward more remarkably than those shown in Fig. 3a. Occasionally, the drifters can make a loop or excursion into the SCS and then turn clockwise back to the Pacific (Fig. 3g), reflecting the path of KCL. This LCS type also exhibits looping FTLE ridges near the Luzon Strait; such a pattern is clearly seen in the FTLE field on December 24, 2003 (Fig. 3c). In this work, in order to quantitatively distinguish the leaping and looping paths of LCSs, only when the FTLE ridges of KCL extend west of 120°E, they have been defined as the looping patterns. The drifter trajectories in the fourth type indicate the outflow of SCS water into the Pacific Ocean (Fig. 3h), and the corresponding LCSs feature the FTLE ridges directed northeastward from the west of Luzon Island to the east of Taiwan Island (Fig. 3d). Previous studies on the upper-ocean exchanges in the Luzon Strait mainly focused on the different patterns of the Kuroshio path (e.g., Centurioni and Niiler, 2004; Caruso et al., 2006; Nan et al., 2011, 2015). Unlike these works, our study clearly reveals the transport pathways based on the LCSs and thus identifies not only three types of patterns associated with Kuroshio, but also the outflowing pattern from the SCS to the Pacific Ocean. The latter one could not be easily distinguished from the leaping pattern in the Eulerian perspective, but has been confirmed by the drifter trajectories and the previous LCS analysis by Huang et al. (2015).

The extracted FTLE ridges provide a more objective Lagrangian view of the flow types than is possible based on altimetric geostrophic current and the sparse *in situ* observation. Thus, the FTLE ridges show better statistics of the seasonal and interannual variations. Figure 4a shows the seasonal mean occurrence rates of these four LCS types during the period 1993–2017. The leaking and outflowing types are closely related to the seasonal reversing monsoon. The leaking LCS are predominant in winter, rapidly weaken in spring, and almost disappear in summer, indicating significant seasonality of the Kuroshio intrusion events into the SCS. In contrast, the outflowing LCSs appear most frequently in summer, but are rarely observed in winter, indicating that the southwesterly monsoon may be favorable for the outflow of surface water from the SCS into the Pacific Ocean. Further, the leaping pattern, which is the most frequently occurring pattern, appears in every season and is especially predominant during spring. It accounts for about two-thirds of all spring LCS patterns for 1993–2017, and it is much more frequent in spring than in the other seasons. The occurrence rate of looping LCSs also shows a larger seasonal contrast during the monsoon transition periods, varying from a minimum of 20.5% in spring to a maximum of 31.6% in autumn. The occurrence probabilities of leaping and looping LCSs do not appear to be controlled by the SCS monsoon but could be presumably attributed to the Kuroshio transport east of Luzon Island, which reaches its seasonal minimum in autumn and maximum in spring (Qiu and Lukas, 1996; Yaremchuk and Qu, 2004). According to the inertial boundary

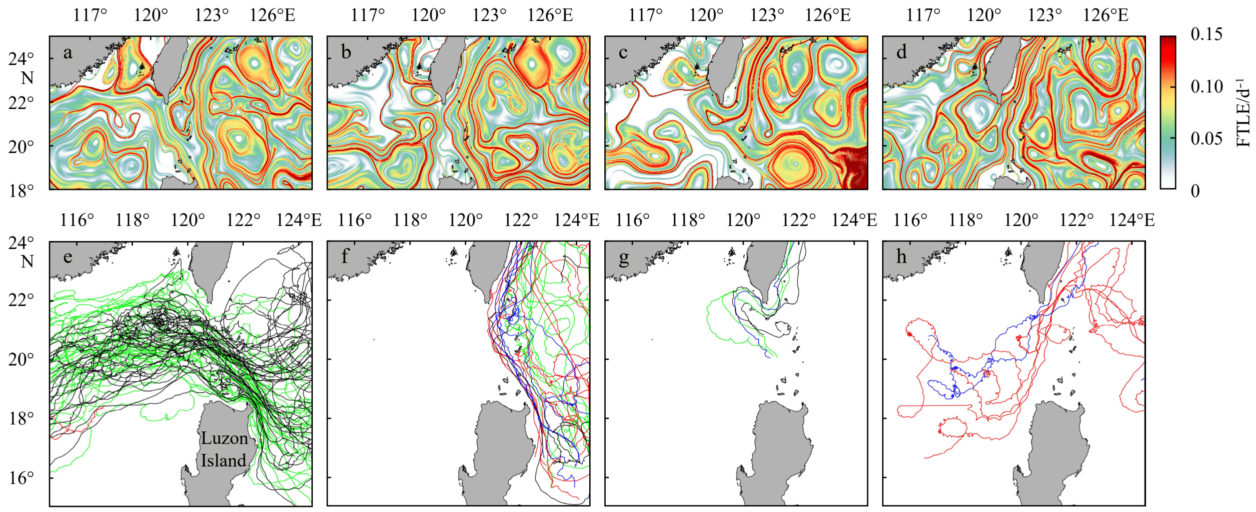

**Fig. 3.** Typical snapshots of FTLE fields for leaking LCS type (March 8, 2003) (a), leaping LCS type (March 31, 2003) (b), looping LCS type (December 24, 2003) (c), outflowing LCS type (June 19, 2000) (d), and the trajectories of the satellite-tracked drifters during the period 2000–2017 corresponding to the four LCS types in a–d (e–h). The green, red, blue and black lines in e–h represent the trajectories in boreal spring, summer, autumn and winter, respectively.

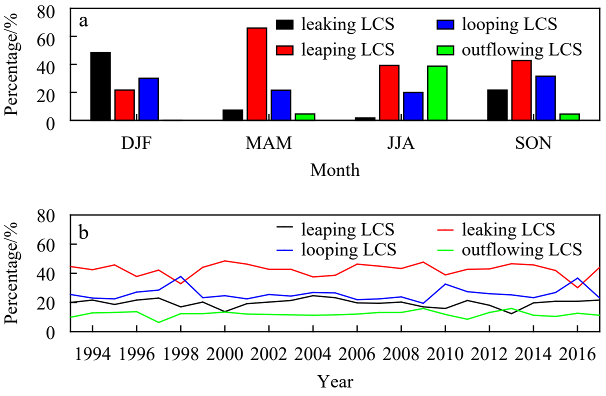

**Fig. 4.** Occurrence rates of four LCS types in each season (a), and each year (b).

current theory proposed by Sheremet (2001), the Kuroshio tends to leap across the Luzon Strait when it is sufficiently strong and shifts to a loop current regime as soon as its transport falls below a certain critical value. Therefore, the stronger (weaker) Kuroshio east of Luzon Island in spring (autumn) season may be in favor of the formations of leaping (looping) LCSs. Despite the strong seasonality of LCS patterns, the regional mean FTLE values at the Luzon Strait (18.5°–22°N, 120°–122°E) have little seasonal difference. This means that it is a challenging work to classify these LCS types by automatic identification algorithms rather than visual recognition, which are worth further studies in the future.

Figure 4b shows the yearly percentages of occurrence for the four LCS types for 1993–2017. The leaping LCSs occur most frequently (probabilities ranging from 30.1% to 48.5%). Another active type is looping LCSs (probabilities ranging from 19.5% to 37.8%), and its occurrence even exceeds that of the leaping type in 1998 and 2016. Among the three LCS types related to Kuroshio flow pattern, the leaking pattern is the rarest and has yearly mean occurrence rates of 12.3%–24.7%. However, the least frequent type among the four types is outflowing LCS type, which accounts for 6.3%–15.9% of the incidence of all types. That is, the Kuroshio dominates the surface water exchanges through the Luzon Strait, and the SCS surface water has much weaker impact on the Kuroshio water east of Luzon Strait. Some previous studies have pointed out that the variations of both Kuroshio and Luzon Strait transports are closely correlated with the El Niño-Southern Oscillation (ENSO) with a time lag of about 4 months (e.g., Qu et al., 2004; Qiu and Chen, 2010). Figure 4b indicates that the occurrences of leaping and looping types are influenced by ENSO as well to some extent. The leaping LCSs occur more frequently than the looping LCSs in most years. However, during the post-El Niño years of 1998 and 2016, the occurrence rates of the looping type exceeded those of the leaping type because of the abrupt increase (decrease) of the looping (leaping) LCSs. These exceptional cases are probably associated with the weakening of Kuroshio after the mature phase of two super El Niño events.

### 3.3 *Lagrangian view of eddy shedding processes*

Some previous *in situ* observations showed that mesoscale eddies originating from the Kuroshio intrusions usually trap the water masses from the Pacific and convey them to the interior SCS (e.g., Wang et al., 2008; Huang et al., 2010). One of the most important eddy formation processes is the detachment of ACEs from the KCL (Li et al., 1998; Nan et al., 2015; Zhang et al., 2017), resembling the ring separation from the Loop Current in the Gulf of Mexico. Previous researches have proved that the combination of LCSs and the released virtual particles can effectively describe the fluid motions under the circumstances of rich eddies (Lehahn et al., 2007; Andrade-Canto et al., 2013). In this study, the LCSs were used along with the tracks of virtual particles to illustrate the eddy-trapping processes of Kuroshio water during the ACE shedding events. The surface geostrophic current shown in Fig. 5a presents a typical KCL pattern to the southwest of Taiwan Island on January 28, 2000. The corresponding FTLE snapshot in Fig. 5b also shows a consistent looping type of attracting LCSs. To corroborate the transport pathways identified in Fig. 5b, we seeded three groups of passive virtual particles at the latitude 18.5°N. The central group was located over the FTLE ridge that directly connected the upstream Kuroshio with the anticyclonic loop, and the other two groups were located 15 km to the east and west of the central one (see the pink, blue, and black dots in Fig. 5b). In each group, 25 virtual particles were released on January 28, and the particle tracks were assessed using a fourth-order Runge-Kutta method. The FTLE snapshots on February 11 and 21 indicated that the KCL gradually enhanced and finally formed a detached ACE (Figs 5c and d). Although the three groups of particles were initially released in the neighboring positions, their trajectories were quite different. The particles in the eastern group migrated northward and leaped across the Luzon Strait, while those in the western group moved along the periphery of the strongest looping FTLE ridge and eventually returned to the western Pacific. Only the particles in the central group entered the interior of the loop along the LCS ridge, circulated anticyclonically, and finally migrated westward with the detached ACE.

To evaluate the overall ability of LCSs in positioning the paths from upstream Kuroshio into the detached ACEs, we conducted virtual particle-tracking experiments for all the 20 eddy shedding events during the period of 1993–2017. In these experiments, the particles were also seeded at the latitude 18.5°N but only within the FTLE ridges extending from the Kuroshio mainstream to the nearest positions of KCL in the SCS. Figure 6a shows an example of the FTLE distribution along the 18.5°N transect on November 25, 2004. We selected the FTLE ridge at ~122.7°E, which reflected the LCS that extended downstream and formed the looping shape near the Luzon Strait (Fig. 7a). Then the particles were released between the troughs on both sides of the LCS (Fig. 6a), within which the zonal FTLE distributions generally exhibited increasing trends and thus stronger convergence toward the central LCS. The initial spacing of the deployed particles is 0.01°. The final ACE detachment was determined by the appearance of the saddle point, that is, an intersection of the attracting and repelling LCSs, between the ACE and the Kuroshio mainstream on December 24, 2004 (Fig. 7d). Since the attracting and repelling LCSs cannot be crossed by particle trajectories, the saddle points

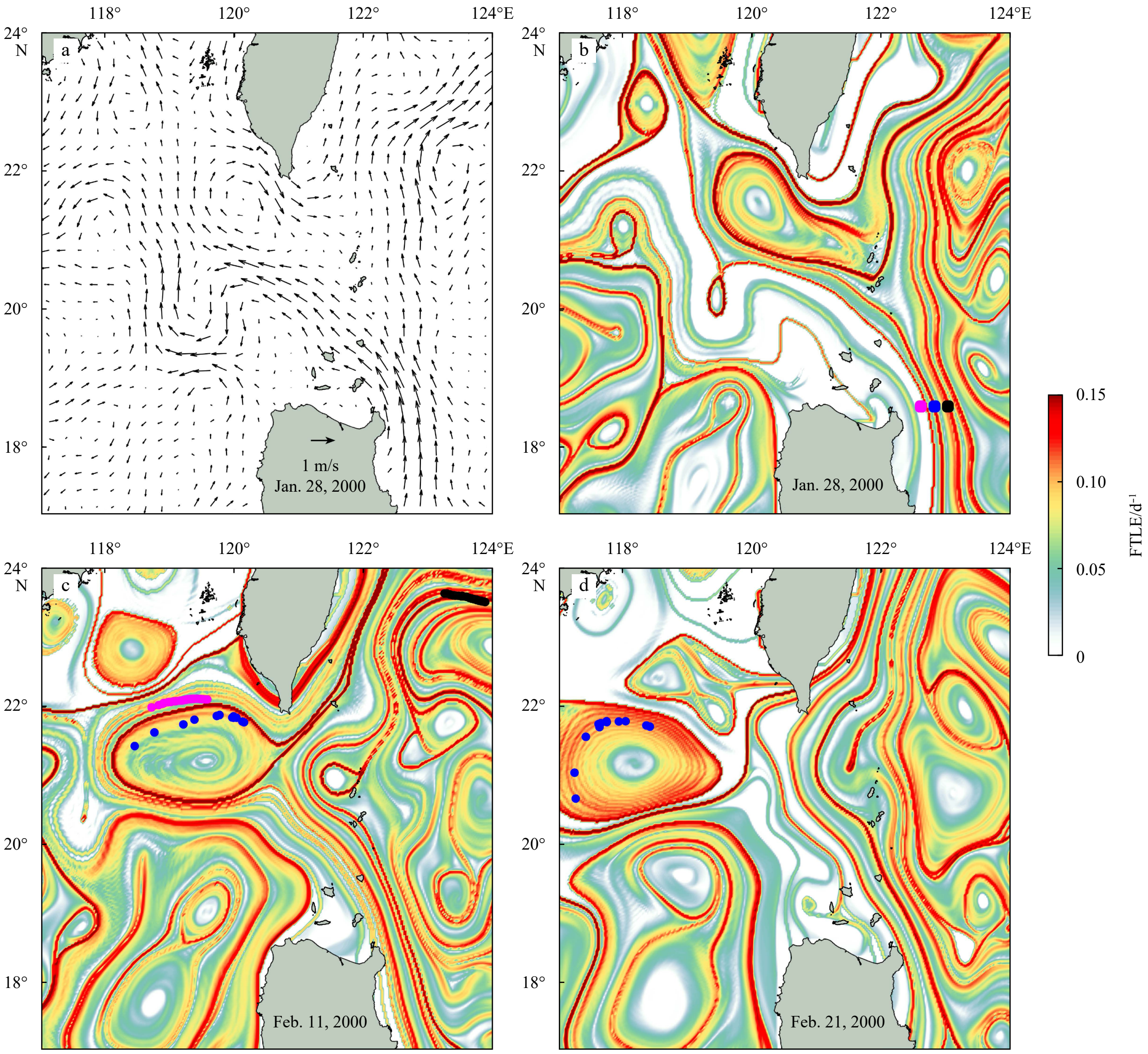

**Fig. 5.** Geostrophic current on January 28, 2000 (a), and snapshots of FTLE fields on January 28 (b), February 11 (c), and February 21 (d), 2000. The instantaneous position of virtual particles are shown by pink, blue, and black dots in b–d.

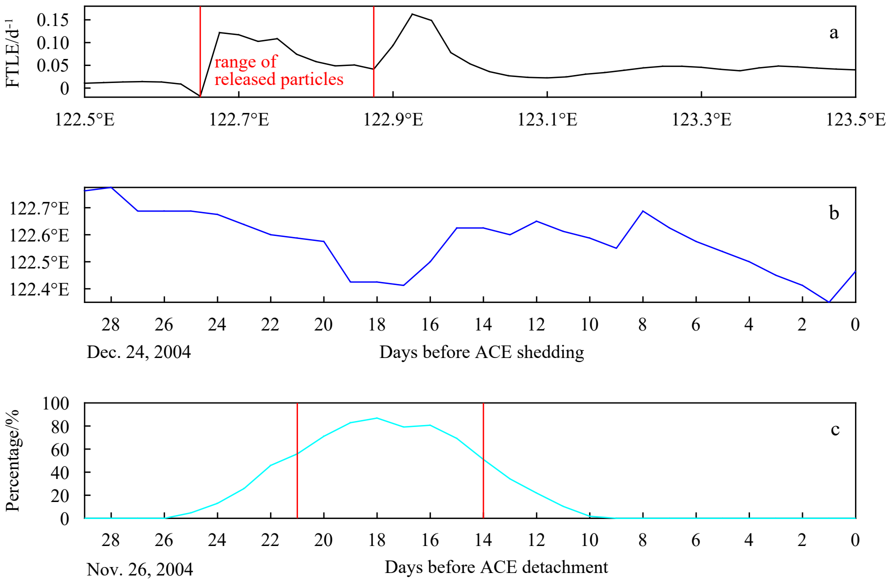

**Fig. 6.** Zonal distribution of FTLE values along the 18.5°N transect on November 25, 2004 (a), mean longitude of the particle released at the 18.5°N transect in 30 d until the date of ACE shedding on December 24, 2004 (b); and the percentages of the daily released particles that finally enter the ACE (c).

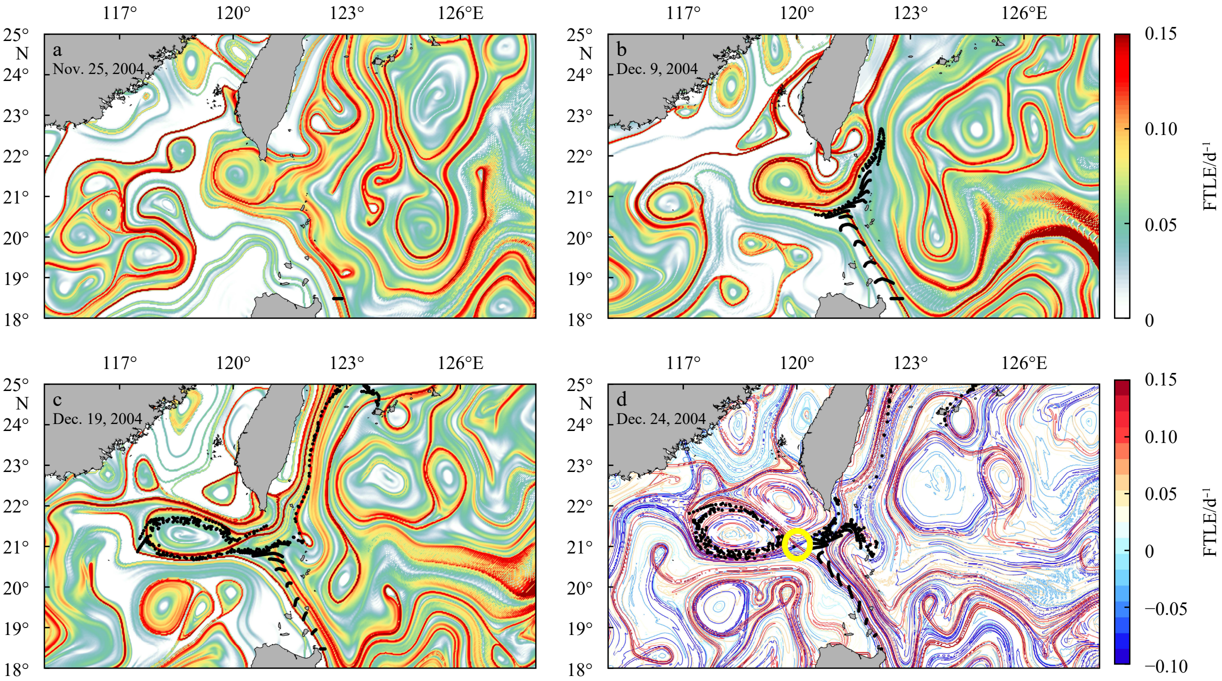

**Fig. 7.** Snapshots of FTLE fields on November 25 (a), December 9 (b), and December 19 (c) and the superposition of FTLE by integrating forward (red) and that by integrating backward (blue) on December 24, 2004 (d). The instantaneous position of the virtual particles are shown by black dots in a–d. The saddle point in d is highlighted by a yellow circle.

defined by their intersections imply that the surrounding water is divided into four relatively independent fluid domains (Haller, 2001). Therefore, these points were also considered an important sign of eddy separation from the mean flow in previous studies (Feng, 2009; Andrade-Canto et al., 2013). In our experiments of 20 eddy shedding events, the particles were released once a day for 30 consecutive days until the separation of the ACE from the Kuroshio. During these periods, the sites for particle release were usually not fixed but varied in the zonal direction because of the movements of the selected FTLE ridges.

During the period of November 25 to December 24, 2004, the mean longitude for particle release showed conspicuous intraseasonal oscillations between 122.3° and 122.8°E (Fig. 6b), reflecting the transient features of the Kuroshio. Figure 6c shows the percentages of daily released particles that were eventually captured by the ACE. The particles released in the initial 6 d (November 25–30) reached the east of KCL in early December. However, because of the relatively weak and unstable nature of the KCL in this stage, most particles directly moved northward, instead of intruding westward into the SCS (Figs 6c, 7a and b). Thereafter, the KCL was gradually enhanced, and the LCSs connecting the upstream Kuroshio with the anticyclonic loop became more robust. Hence, the particles released in the next 12 d (December 1–12) migrated into the KCL and were partly trapped by the finally separated ACE. Note that it took about 7–8 d for the particles in this experiment to move from the deployment sites at 18.5°N to the KCL. Thus, the eddy trapping mainly occurred in the period of December 8–20 because of the time lags of 7–8 d between the release of particles and their arrival at the KCL. The capture ratios exceeded 50% for the particles released on December 3–10, indicating the high eddy-trapping efficiency in mid-December (Figs 6c and 7c). In particular, more than 70% of the particles released during December 4–7 were entrained into the detached eddy. The particles released during December 13–24 arrived at the east of the KCL after December 20. At this time, the KCL had further moved westward, formed a relatively isolated vortex, and eventually detached from the Kuroshio. The eddy detachment, as indicated by the saddle point of the attracting and repelling LCSs, occurred on December 24 (Fig. 7d). In this period, particles could no longer enter the SCS but leap northward across the Luzon Strait (Figs 6c and 7d). The above particle-tracking experiment suggests that to some extent, the LCSs can be used to predict the locations of the upstream Kuroshio waters captured by the detached eddies about 7–8 d in advance.

The particle-tracking experiments of all 20 ACE shedding events from 1993 to 2017 showed that the eddy trapping of virtual particles occurred in 18 cases. Most of these events were also recognized in the altimeter sea level data (Zhang et al., 2017), validating again the feasibility of LCSs in identifying the ACE shedding events. Similar to the situation shown in Fig. 6c, the capture ratios in the other 16 experiments had a predominant peak, first increasing from zero and then decreasing to zero (Fig. 8). However, the peaking time and maximum values show large diversities in these experiments. For instance, the earliest peaking time occurred 23 d before the eddy separation in February 2004, while the latest peaking time occurred 7 d before the eddy separation in December 2015. The maximum ratio in the March 2001 event was only 13%, which is the lowest peak observed in these experiments. In contrast, the ratios in some other cases (e.g., March 2001, December 2006, and February 2017) peaked at 100%, indicative of the strong trapping effects of these ACEs. The result for January 1993 is an obvious exception from the 18 experiments. In this case, more than half of the particles released in the initial 2 d were captured by the ACE, indicating that its eddy trapping occurred much earlier than the processes in the other 17 cases. The above diversities in eddy-trapping characteristics are probably caused by the strong flow nonlinearity during the KCL evolutions.

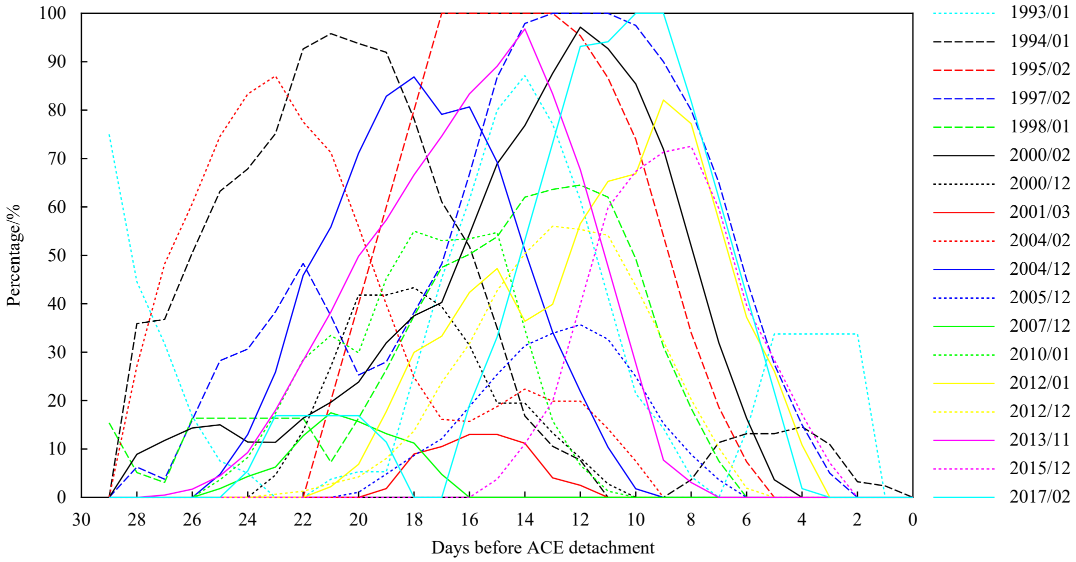

**Fig. 8.** Percentages of the daily released particles that finally enter the ACEs in 18 ACE shedding events with eddy trapping during the period of 1993–2017.

In addition to the above 18 cases, two other ACE shedding events were observed in December 2006, and October 2015. A common feature in both events was that there existed a cold eddy to the south of the KCL with the size and intensity comparable to those of KCL. With the eddy shedding from KCL, the ACE and CE eventually formed a meridional eddy dipole to the west of the Luzon Strait. Here, we consider the case of October 2015 as an example. As shown in Fig. 9a, the confluence of KCL and CE resulted in a westward flowing jet current at the central Luzon Strait. The corresponding FTLE ridges did not show the looping LCS, a typical pattern seen in most eddy shedding events. Instead, under the influence of CE, the LCSs, including the one closest to the KCL, displayed leaking paths connecting the upstream Kuroshio with the interior SCS through the westward flowing jet (Fig. 9b). The relevant particle-tracking experiments showed that the upstream particles mostly entered the interior SCS through the leaking LCS paths instead of being captured by the ACEs, which validated from another side the accuracy of the transport pathways described by LCSs.

### 3.4 *Weak exchanges between CEs and the Kuroshio*

Another interesting situation is the existence of a single CE northwest of the Luzon Strait, as shown in the typical example for May 4, 2017 (Fig. 9c). Such a flow pattern was considered in some previous studies as a cyclonic loop, one of the important types of Kuroshio intrusions (Caruso et al., 2006). However, the corres-

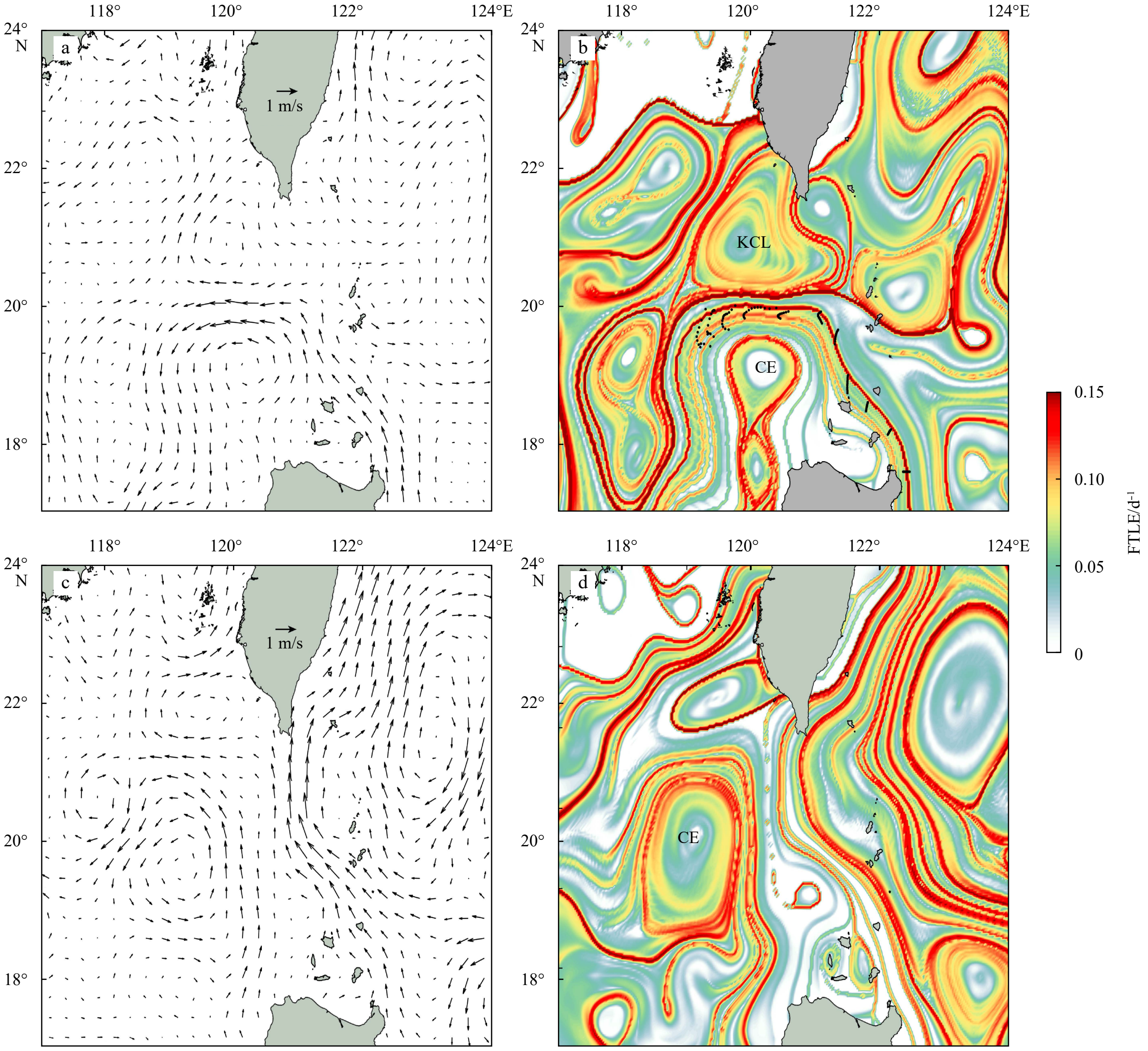

**Fig. 9.** Surface geostrophic current (a) and snapshot of the FTLE field (b) on October 26, 2015. Surface geostrophic current (c) and snapshot of FTLE field (d) on May 4, 2017.

ponding LCSs exhibited obvious transport barriers separating the CE from the Kuroshio mainstream (Fig. 9d). In the period of 1993–2017, the LCS patterns similar to Fig. 9d persisted throughout the lifetimes of all CEs west of the Luzon Strait (figures not shown). The lack of transport pathways between CEs and the Kuroshio means that the water masses captured by CEs were not directly supplied by the waters from the western Pacific.

Cruise observations of an ACE in January 2010 and a CE in May 2017 were used to further illustrate their differences in water masses. Both eddies originated near the Luzon Strait. The *in situ* data are briefly introduced in Section 2.1, and the details of these two eddies are described by Liu et al. (2013) and Huang et al. (2019). Although the sampling location of CE is closer to the Luzon Strait than that of ACE, the *T*-*S* properties show that the CE-trapped water is fresher and resembles the SCS climatology to a greater extent, while the ACE-trapped water is saltier and more similar to the climatological Pacific water (Fig. 10). The contrasting water properties in the centers of the CE and ACE could be well explained by the differences in their water exchanges with the Kuroshio, as inferred from the LCS snapshots.

## 4 Discussion and summary

Upper-ocean circulation around the Luzon Strait exhibits strong spatiotemporal variability because of the complex bathymetry and active Kuroshio-eddy interactions. Therefore, it is often difficult to determine the water exchange characteristics in the Luzon Strait solely by means of the flow fields. In this study, the FTLE fields hidden in surface ocean current were derived by calculating the expansion or contraction rates for neighboring passive fluid particles. The LCSs extracted as ridges in the FTLE fields can be categorized into four major patterns of transport pathways in the vicinity of the Luzon Strait: the leaking, leaping, looping, and outflowing types. Unlike some previous studies that classified the Kuroshio path near the Luzon Strait (e.g., Centurioni and Niiler, 2004; Caruso et al., 2006; Nan et al., 2011, 2015), this study identifies not only three LCS types associated with the Kuroshio variability, but also the LCS type that flows from the SCS to the Pacific Ocean.

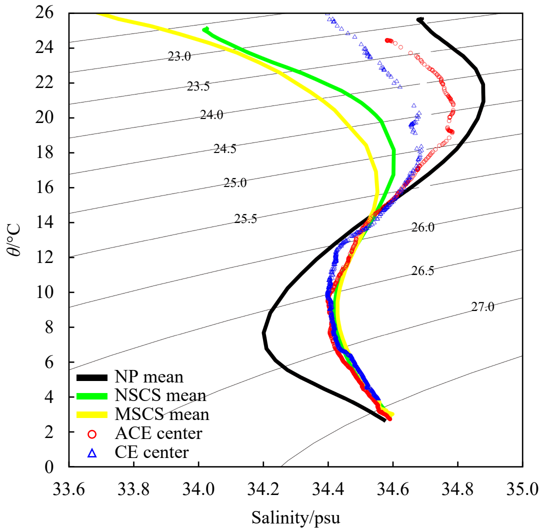

**Fig. 10.** *T*-*S* diagrams of the conductivity-temperature-depth (CTD) profiles at the centers of an ACE in January 2010 (red) and a CE in May 2017 (blue). The climatological annual mean *T*-*S* diagrams in the northern SCS (green line), middle SCS (yellow line), and northwest Pacific Ocean (black line) are derived from the World Ocean Atlas 2005 dataset, and averaged in the regions shown in inset of Fig. 1.

The occurrences of all these LCSs show significant seasonal variations. The leaping type, which is the most frequent one, appears in every season and is the most active in spring. The leaking and outflowing types are both sensitive to the monsoon reversal and occur most frequently in winter and summer, respectively. The looping type shows the weakest seasonality with comparable occurrence rates in all four seasons. With regard to the yearly occurrence rates, the leaping type occurs more frequently than the other three types in most years. However, in 1998 and 2016, the decay years of super El Niño events, the leaping type was surpassed by the looping type, potentially indicating the modulations of ENSO.

The water exchanges during the ACE separations from KCL were further analyzed with the synergy of LCSs and particle-tracking experiments. In the 20 eddy shedding events during 1993–2017, we selected the FTLE ridges extending from the Kuroshio mainstream to the nearest positions of KCL in the SCS and then released virtual particles within the FTLE ridges at 18.5°N. The particles were continuously released for 30 d until ACE detachment from the KCL. In 18 eddy shedding events with evident looping LCS patterns, the released particles were partly captured by the detached ACEs. However, the capture ratios and timespans varied significantly among these experiments. Such large diversities in eddy-trapping processes may be attributed to the strong nonlinear nature of the Kuroshio and KCL. In the remaining two ACE shedding events, a strong CE was observed to the south of the KCL. The corresponding LCSs displayed the leaking type along the westward flowing jet current between the CE and the KCL. Instead of being captured by the ACEs, most of the particles released at 18.5°N directly entered the interior SCS through the leaking paths.

When there was only one CE west of the Luzon Strait, the corresponding LCSs clearly divided the CE and the Kuroshio into different fluid domains. The strong transport barriers along the Luzon Strait indicate that the cyclonic loop proposed in previous studies (e.g., Caruso et al., 2006) may not be the effective path for the Kuroshio intrusions into the SCS. The different origins of CE- and ACE-trapped waters were also supported by the distinct *T*-*S* properties in eddy centers.

This work demonstrates that the FTLE or similar Lagrangian approaches are adequate and reliable for elucidating the transport characteristics in the vicinity of Luzon Strait. In particular, the transport information provided by LCSs is helpful to better understand and predict the water exchanges between eddies and the Kuroshio in different eddy configurations. However, the prediction skills for eddy-induced transports are still challenged and limited by the large diversities in eddy activities. For instance, the events with longer winding time of KCL or ACE and relative faster variability of flow pattern would not be reasonably predicted by the LCSs. For improving the LCS-based prediction skills, it is necessary to further clarify the underlying dynamics of the Kuroshio-eddy interactions.

### *Acknowledgements*

The surface geostrophic current data used in this study are released by the CEMES (http://marine.copernicus.eu/services-portfolio/access-toproducts). The satellite-tracked drifter data are obtained from the NOAA/AOML Drifter Data Assembly Center (ftp://ftp.aoml.noaa.gov/phod/pub/pazos/data/hur/dac.html).

### References

Andrade-Canto F, Sheinbaum J, Sansón L Z. 2013. A Lagrangian approach to the Loop Current eddy separation. Nonlinear Processes in Geophysics, 20(1): 85–96, doi: 10.5194/npg-20-85-2013

Beron-Vera F J, Olascoaga M J, Goni G J. 2008. Oceanic mesoscale eddies as revealed by Lagrangian coherent structures. Geophysical Research Letters, 35(12): L12603, doi: 10.1029/2008GL033957

Branicki M, Wiggins S. 2009. Finite-time Lagrangian transport analysis: stable and unstable manifolds of hyperbolic trajectories and finite-time Lyapunov exponent. Nonlinear Processes in Geophysics, 17(1): 1–36

Caruso M J, Gawarkiewicz G G, Beardsley R C. 2006. Interannual variability of the Kuroshio intrusion in the South China Sea. Journal of Oceanography, 62(4): 559–575, doi: 10.1007/s10872-006-0076-0

Centurioni L R, Niiler P P, Lee D K. 2004. Observations of inflow of Philippine Sea surface water into the South China Sea through the Luzon Strait. Journal of Physical Oceanography, 34(1): 113–121, doi: 10.1175/1520-0485(2004)034<0113:OOIOPS>2.0.CO;2

Chu P C, Li Rongfeng. 2000. South China Sea isopycnal-surface circulation. Journal of Physical Oceanography, 30(9): 2419–2438, doi: 10.1175/1520-0485(2000)030<2419:SCSISC>2.0.CO;2

D'Ovidio F, Fernández V, Hernández-García E, et al. 2004. Mixing structures in the Mediterranean Sea from finite-size Lyapunov exponents. Geophysical Research Letters, 31(17): L17203

Fang Guohong, Wang Yonggang, Wei Zexun, et al. 2009. Interocean circulation and heat and freshwater budgets of the South China Sea based on a numerical model. Dynamics of Atmospheres and Oceans, 47(1–3): 55–72, doi: 10.1016/j.dynatmoce.2008.09.003

Feng Ming. 2009. Eddy-induced cross-shelf phytoplankton transport along the downwelling coast off Western Australia. Journal of Tropical Oceanography, (5): 6–10

Gordon A L, Huber B A, Metzger E J, et al. 2012. South China Sea throughflow impact on the Indonesian throughflow. Geophysical Research Letters, 39(11): L11602, doi: 10.1029/2012GL052021

Haller G. 2001. Lagrangian structures and the rate of strain in a partition of two-dimensional turbulence. Physics of Fluids, 13(11): 3365–3385, doi: 10.1063/1.1403336

Haller G. 2015. Lagrangian coherent structures. Annual Review of Fluid Mechanics, 47: 137–162, doi: 10.1146/annurev-fluid-010313-141322

Haller G, Yuan Guocheng. 2000. Lagrangian coherent structures and mixing in two-dimensional turbulence. Physica D: Nonlinear Phenomena, 147(3–4): 352–370

Harrison C S, Glatzmaier G A. 2010. Lagrangian coherent structures in the California Current System—sensitivities and limitations. Geophysical & Astrophysical Fluid Dynamics, 106(1): 22–44, doi: 10.1080/03091929.2010.532793

Huang Bangqin, Hu Jun, Xu Hongzhou, et al. 2010. Phytoplankton community at warm eddies in the northern South China Sea in winter 2003/2004. Deep Sea Research Part Ⅱ: Topical Studies in Oceanography, 57(19–20): 1792–1798

Huang Gaolong, Wei Xing, Zhan Haigang. 2015. Lagrangian analysis of drifter trajectories near the Luzon Strait. Journal of Tropical Oceanography (in Chinese), 34(1): 15–22

Huang Zhida, Zhuang Wei, Hu Jianyu, et al. 2019. Observations of the Luzon Cold Eddy in the northeastern South China Sea in May 2017. Journal of Oceanography, 75(5): 415–422, doi: 10.1007/s10872-019-00510-z

Huhn F, Von Kameke A, Allen-Perkins S, et al. 2012. Horizontal Lagrangian transport in a tidal-driven estuary—Transport barriers attached to prominent coastal boundaries. Continental Shelf Research, 39–40: 1–13, doi: 10.1016/J.CSR.2012.03.005

Jia Yinglai, Chassignet E P. 2011. Seasonal variation of eddy shedding from the Kuroshio intrusion in the Luzon Strait. Journal Oceanography, 67: 601–611, doi: 10.1007/s10872-011-0060-1

Lehahn Y, d'Ovidio F, Lévy M, et al. 2007. Stirring of the northeast Atlantic spring bloom: A Lagrangian analysis based on multisatellite data. Journal of Geophysical Research, 112(C8): C08005

Li Li, Nowlin W D Jr, Su Jilan. 1998. Anticyclonic rings from the Kuroshio in the South China Sea. Deep Sea Research Part I: Oceanographic Research Papers, 45(9): 1469–1482, doi: 10.1016/S0967-0637(98)00026-0

Li Jiaxun, Zhang Ren, Jin Baogang. 2011. Eddy characteristics in the northern South China Sea as Inferred from lagrangian drifter data. Ocean Science, 7(5): 661–669, doi: 10.5194/os-7-661-2011

Lian Zhan, Sun Baonan, Wei Zexun, et al. 2019. Comparison of eight detection algorithms for the quantification and characterization of mesoscale eddies in the South China Sea. Journal Atmospheric and Oceanic Technology, 36(7): 1361–1380, doi: 10.1175/JTECH-D-18-0201.1

Liu Changjian, Du Yan, Zhuang Wei, et al. 2013. Evolution and propagation of a mesoscale eddy in the northern South China Sea during winter. Acta Oceanologica Sinica, 32(7): 1–7, doi: 10.1007/s13131-013-0325-1

Lumpkin R, Johnson G C. 2013. Global ocean surface velocities from drifters: Mean, variance, El Niño-Southern Oscillation response, and seasonal cycle. Journal of Geophysical Research: Oceans, 118(6): 2992–3006, doi: 10.1002/Jgrc.20210

Metzger E J, Hurlburt H E. 2001. The nondeterministic nature of Kuroshio penetration and eddy shedding in the South China Sea. Journal of Physical Oceanography, 31(7): 1712–1732, doi: 10.1175/1520-0485(2001)031<1712:TNNOKP>2.0.CO;2

Nan Feng, Xue Huijie, Chai Fei, et al. 2011. Identification of different types of Kuroshio intrusion into the South China Sea. Ocean Dynamics, 61(9): 1291–1304, doi: 10.1007/s10236-011-0426-3

Nan Feng, Xue Huijie, Yu Fei. 2015. Kuroshio intrusion into the South China Sea: A review. Progress in Oceanography, 137: 314–333, doi: 10.1016/j.pocean.2014.05.012

Peacock T, Haller G. 2013. Lagrangian coherent structures: The hidden skeleton of fluid flows. Physics Today, 66(2): 41–47, doi: 10.1063/PT.3.1886

Pujol M I, Faugère Y, Taburet G, et al. 2016. DUACS DT2014: The new multi-mission altimeter data set reprocessed over 20 years. Ocean Science, 12(5): 1067–1090, doi: 10.5194/os-12-1067-2016

Qian Yukun, Peng Shiqiu, Li Yineng. 2013. Eulerian and lagrangian statistics in the South China Sea as deduced from surface drifters. Journal of Physical Oceanography, 43(4): 726–743, doi: 10.1175/JPO-D-12-0170.1

Qiu Bo, Chen Shuiming. 2010. Interannual-to-decadal variability in the bifurcation of the North equatorial current off the Philippines. Journal of Physical Oceanography, 40(11): 2525–2538, doi: 10.1175/2010JPO4462.1

Qiu Bo, Lukas R. 1996. Seasonal and interannual variability of the North Equatorial Current, the Mindanao Current, and the Kuroshio along the Pacific western boundary. Journal of Geophysical Research: Oceans, 101(C5): 12315–12330, doi: 10.1029/95JC03204

Qiu Chunhua, Mao Huabin, Liu Hailong, et al. 2019. Deformation of a warm eddy in the northern South China Sea. Journal of Geophysical Research: Oceans, 124(8): 5551–5564, doi: 10.1029/2019JC015288

Qu Tangdong, Du Yan, Meyers G, et al. 2005. Connecting the tropical Pacific with Indian Ocean through South China Sea. Geophysical Research Letters, 32(24): L24609, doi: 10.1029/2005GL024698

Qu Tangdong, Du Yan, Sasaki H. 2006. South China Sea throughflow: A heat and freshwater conveyor. Geophysical Research Letters, 33(23): L23617, doi: 10.1029/2006GL028350

Qu Tangdong, Kim Y Y, Yaremchuk M, et al. 2004. Can Luzon Strait transport play a role in conveying the impact of ENSO to the South China Sea. Journal of Climate, 17(18): 3644–3657, doi: 10.1175/1520-0442(2004)017<3644:CLSTPA>2.0.CO;2

Qu Tangdong, Mitsudera H, Yamagata T. 2000. Intrusion of the North Pacific Waters into the South China Sea. Journal of Geophysical Research: Oceans, 105(C3): 6415–6424, doi: 10.1029/1999JC900323

Shadden S C, Lekien F, Marsden J E. 2005. Definition and properties of Lagrangian coherent structures from finite-time Lyapunov exponents in two-dimensional aperiodic flows. Physica D: Nonlinear Phenomena, 212(3–4): 271–304

Shaw P T. 1991. The seasonal variation of the intrusion of the Philippine Sea water into the South China Sea. Journal of Geophysical Research: Oceans, 96(C1): 821–827, doi: 10.1029/90JC02367

Sheremet V A. 2001. Hysteresis of a western boundary current leaping across a gap. Journal of Physical Oceanography, 31(5): 1247–1259, doi: 10.1175/1520-0485(2001)031<1247:HOAWBC>2.0.CO;2

Wang Dongxiao, Liu Qinyan, Huang Ruixin, et al. 2006. Interannual variability of the South China Sea throughflow inferred from wind data and an ocean data assimilation product. Geophysical Research Letters, 33(14): L14605, doi: 10.1029/2006GL026316

Wang Xiaowei, Liu Zhiyu, Peng Shiqiu. 2017. Impact of tidal mixing on water mass transformation and circulation in the South China Sea. Journal of Physical Oceanography, 47(2): 419–432, doi: 10.1175/JPO-D-16-0171.1

Wang Huizan, Liu Quanhong, Yan Hengqian, et al. 2019. The interactions between surface Kuroshio transport and the eddy field east of Taiwan using satellite altimeter data. Acta Oceanologica Sinica, 38(4): 116–125, doi: 10.1007/s13131-019-1417-3

Wang Guihua, Su Jilan, Chu P C. 2003. Mesoscale eddies in the South China Sea observed with altimeter data. Geophysical Research Letters, 30(21): 2121, doi: 10.1029/2003GL018532

Wang Dongxiao, Xu Hongzhou, Lin Jing, et al. 2008. Anticyclonic eddies in the northeastern South China Sea during winter 2003/2004. Journal of Oceanography, 64(6): 925–935, doi: 10.1007/s10872-008-0076-3

Wei Zexun, Li Shujiang, Susanto R D, et al. 2019. An overview of 10-year observation of the South China Sea branch of the Pacific to Indian Ocean throughflow at the Karimata Strait. Acta Oceanologica Sinica, 38(4): 1–11, doi: 10.1007/s13131-019-1410-x

Wei Xin, Zhan Haigang, Cai Shuqun, et al. 2018. Detecting the transport barriers in the Pearl River estuary, Southern China with the aid of Lagrangian coherent structures. Estuarine, Coastal and Shelf Science, 205: 10–20, doi: 10.1016/j.ecss.2018.03.010

Wiggins S. 2005. The dynamical systems approach to lagrangian transport in oceanic flows. Annual Review of Fluid Mechanics, 37: 295–328, doi: 10.1146/annurev.fluid.37.061903.175815

Xue Huijie, Chai Fei, Pettigrew N, et al. 2004. Kuroshio intrusion and the circulation in the South China Sea. Journal of Geophysical

Research, 109(C2): C02017

Yaremchuk M, Qu Tangdong. 2004. Seasonal variability of the large-scale currents near the coast of the Philippines. Journal of Physical Oceanography, 34(4): 844–855, doi: 10.1175/1520-0485(2004)034<0844:SVOTLC>2.0.CO;2

Yuan Dongliang, Han Weiqing, Hu Dunxin. 2006. Surface Kuroshio path in the Luzon Strait area derived from satellite remote sensing data. Journal of Geophysical Research: Oceans, 111(C11): C11007, doi: 10.1029/2005JC003412

Zhang Zhiwei, Zhao Wei, Qiu Bo, et al. 2017. Anticyclonic eddy sheddings from Kuroshio loop and the accompanying cyclonic eddy in the northeastern South China Sea. Journal of Physical Oceanography, 47(6): 1243–1259, doi: 10.1175/JPO-D-16-0185.1

Zheng Quanan, Ho Chungru, Xie Lingling, et al. 2019. A case study of a Kuroshio main path cut-off event and impacts on the South China Sea in fall-winter 2013–2014. Acta Oceanologica Sinica, 38(4): 12–19, doi: 10.1007/s13131-019-1411-9

Zhu Jia, Zheng Quanan, Hu Jianyu, et al. 2019. Classification and 3-D distribution of upper layer water masses in the northern South China Sea. Acta Oceanologica Sinica, 38(4): 126–135, doi: 10.1007/s13131-019-1418-2

Zhuang Wei, Xie Shangping, Wang Dongxiao, et al. 2010. Intraseasonal variability in sea surface height over the South China Sea. Journal of Geophysical Research: Oceans, 115(C4): C04010, doi: 10.1029/2009JC005647